Naval Research Laboratory

Washington, DC 20375-5320

NRL/MR/5652--07-9065

Laser Noise and Its Impact on the Performance of Intensity-Modulation with Direct-Detection Analog Photonic Links

VINCENT J. URICK
PREETPAUL S. DEVGAN
JASON D. MCKINNEY
JAMES L. DEXTER

Photonics Technology Branch
Optical Sciences Division

August 10, 2007

REPORT DOCUMENTATION PAGE

Form Approved
OMB No. 0704-0188

1. REPORT DATE *(DD-MM-YYYY)*	2. REPORT TYPE	3. DATES COVERED *(From - To)*
10-08-2007	Memorandum Report	01-10-2006 – 08-01-2007

4. TITLE AND SUBTITLE

Laser Noise and Its Impact on the Performance of Intensity-Modulation with Direct-Detection Analog Photonic Links

5a. CONTRACT NUMBER

5b. GRANT NUMBER

5c. PROGRAM ELEMENT NUMBER

6. AUTHOR(S)

Vincent J. Urick, Preetpaul S. Devgan, Jason D. McKinney, and James L. Dexter

5d. PROJECT NUMBER

5e. TASK NUMBER

5f. WORK UNIT NUMBER

7. PERFORMING ORGANIZATION NAME(S) AND ADDRESS(ES)

Naval Research Laboratory, Code 5652
4555 Overlook Avenue, SW
Washington, DC 20375-5320

8. PERFORMING ORGANIZATION REPORT NUMBER

NRL/MR/5652--07-9065

9. SPONSORING / MONITORING AGENCY NAME(S) AND ADDRESS(ES)

Office of Naval Research
One Liberty Center
875 North Randolph Street
Arlington, VA 22203-1995

10. SPONSOR / MONITOR'S ACRONYM(S)

ONR

11. SPONSOR / MONITOR'S REPORT NUMBER(S)

12. DISTRIBUTION / AVAILABILITY STATEMENT

Approved for public release; distribution is unlimited.

13. SUPPLEMENTARY NOTES

14. ABSTRACT

The equations for radio-frequency gain, radio-frequency noise figure, compression dynamic range and spurious-free dynamic range are derived for an analog photonic link employing intensity modulation and direct detection. In particular, the impact of laser noise on the performance of an analog photonic link is demonstrated in terms of these metrics. We describe the experimental procedure for measuring laser noise and the measured laser noise spectra of lasers suitable for analog photonics are shown.

15. SUBJECT TERMS

Long haul fiber optic link
Analog photonics
Fiber amplifiers
Spurious-free dynamic range

16. SECURITY CLASSIFICATION OF:			17. LIMITATION OF ABSTRACT	18. NUMBER OF PAGES	19a. NAME OF RESPONSIBLE PERSON
a. REPORT	b. ABSTRACT	c. THIS PAGE			Vincent J. Urick
Unclassified	Unclassified	Unclassified	UL	24	19b. TELEPHONE NUMBER *(include area code)* (202) 767-9352

Standard Form 298 (Rev. 8-98)
Prescribed by ANSI Std. Z39.18

TABLE OF CONTENTS

LASER NOISE AND ITS IMPACT ON THE PERFORMANCE OF INTENSITY-MODULATION WITH DIRECT-DETECTION ANALOG PHOTONIC LINKS

EXECUTIVE SUMMARY

- The equations for radio-frequency gain, radio-frequency noise figure, compression dynamic range and spurious-free dynamic range are derived for an analog photonic link employing intensity modulation and direct detection.
- The impact of laser noise on the above-referenced performance metrics is derived.
- The procedure for measuring laser noise is demonstrated.
- The measured laser noise spectra of lasers suitable for analog photonics are shown.

Manuscript approved June 14, 2007.

LASER NOISE AND ITS IMPACT ON THE PERFORMANCE OF INTENSITY-MODULATION WITH DIRECT-DETECTION ANALOG PHOTONIC LINKS

1 INTRODUCTION

Photonics offers numerous advantages over traditional radio-frequency (RF) hardware for various analog applications. Such advantages include decreased size and weight, increased flexibility, invulnerability to electromagnetic interference, larger bandwidth in fiber and decreased signal loss in fiber. Long-haul analog applications such as antenna remoting [1],[2], radio over fiber [1] and optoelectronic oscillators [3] benefit from the very low signal loss in fiber, typically 0.5 dB/km in any RF band. Short-reach applications of analog photonics include wideband signal processing and manipulation for electromagnetic warfare and radar demands [4],[5]. In addition, analog photonics has proven useful for other arrayed-radar [6],[7] applications. In all of the above examples and in any other analog photonic application, the noise due to the lasers involved is of the utmost importance.

In this report, we will quantitatively demonstrate the effects that laser noise has on an analog photonic system. The metrics that completely describe an analog photonic system, namely, RF gain, RF noise figure, compression dynamic range and spurious-free dynamic range, will be derived for an intensity-modulation direct-detection format in Section 2. These metrics are derived in general with special attention paid to the impact that laser noise has on the performance. In Section 3, the experimental procedure for measuring laser noise will be demonstrated in detail. The results of noise measurements on lasers that are suitable for analog-photonic applications will be given in Section 4 and the report is concluded in Section 5. This report is brief but self-contained, assuming a vague familiarity with analog systems and photonics.

2 IMDD PERFORMANCE METRICS

Here we derive the RF gain, RF noise figure, compression dynamic range and spurious-free dynamic range for an analog photonic link employing intensity-modulation with direct-detection (IMDD). The impact of laser power and noise on these performance metrics is demonstrated explicitly.

The IMDD architecture is shown in Fig. 1 and consists of a transmit laser, a push-pull $LiNbO_3$ Mach-Zehnder modulator (MZM) and a p-i-n photodiode. The analog signal and DC bias at the MZM input comprise the total drive voltage for the photonic link. As will be detailed below, this drive voltage induces a phase shift on the optical electric field as it traverses the electrooptic $LiNbO_3$ material, which is converted into amplitude modulation in the interferometric configuration such that it can be demodulated with the photodiode. Note that the development here assumes a push-pull, or balanced, MZM (an unbalanced MZM yields a different optical field but the same RF performance).

The mathematical analysis of the link in Fig. 1 is carried out in the time domain. We first write the electric field at the laser output as $E_{\text{in}}(t) = \kappa\sqrt{2P_{\text{o,in}}}\,e^{i\omega_0 t}$, where $P_{\text{o,in}}$ is the optical power at angular frequency ω_0. Here κ is a constant relating optical field and optical power such that $P_{\text{o,in}} = E_{\text{in}}^{*}E_{\text{in}}/(2\kappa^2)$. Next, we represent the drive voltage as $V_{\text{drive}}(t) = V_{\text{dc}} + V_{\text{rf}}\sin\Omega t$, where V_{dc} is the DC bias voltage, V_{rf} is the analog voltage amplitude and the

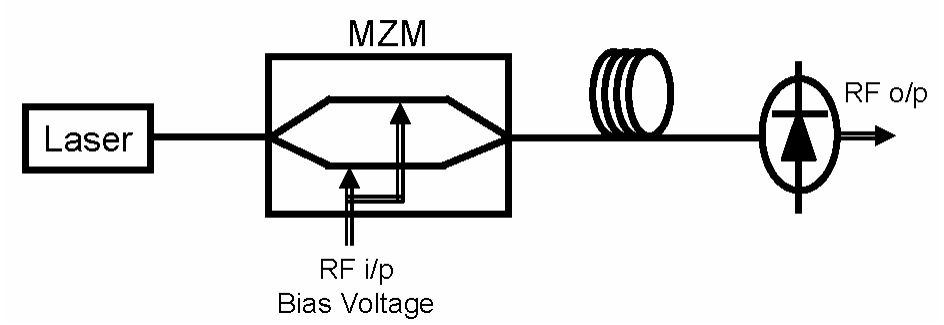

Fig. 1. Intensity modulation with direct detection photonic link employing a laser, Mach-Zehnder modulator (MZM) and p-i-n photodiode.

analog drive frequency is $f_{\rm rf} = \Omega/2\pi$. In the push-pull configuration, this drive voltage produces a phase shift of $\phi(t) = \phi_{\rm dc}/2 + (\phi_{\rm rf}/2)\sin\Omega t$ in one arm of the MZM and $-\phi(t)$ in the other arm, where $\phi_{\rm dc}$ is the phase shift due to the DC bias and $\phi_{\rm rf}$ the amplitude of the sinusoidal phase shift. The static and analog phase shifts are related to the drive voltage by $\phi_{\rm dc} = \pi(V_{\rm dc}/V_{\pi,\rm dc})$ and $\phi_{\rm rf} = \pi(V_{\rm rf}/V_{\pi,\rm rf})$ where V_π is the voltage required to produce a phase shift of π radians. Note that V_π is a frequency-dependent characteristic of the $LiNbO_3$ MZM that quantifies how well voltage is converted to an index change through the electrooptic effect. Assuming ideal 50/50 coupling at the input and output of the MZM, the electric fields at the output of the MZM can be calculated using

$$\begin{bmatrix} E_1(t) \\ E_2(t) \end{bmatrix} = \frac{\sqrt{\alpha_{\rm mzm}}}{2} \begin{bmatrix} 1 & i \\ i & 1 \end{bmatrix} \begin{bmatrix} e^{i\phi(t)} & 0 \\ 0 & e^{-i\phi(t)} \end{bmatrix} \begin{bmatrix} 1 & i \\ i & 1 \end{bmatrix} \begin{bmatrix} E_{\rm in}(t) \\ 0 \end{bmatrix} \tag{1}$$

where $\alpha_{\rm mzm}$ is the optical power loss factor for the MZM. Carrying out the transfer of the MZM (1), we then have

$$\begin{bmatrix} E_1(t) \\ E_2(t) \end{bmatrix} = \frac{\kappa}{2}\sqrt{2\alpha_{\rm mzm}P_{\rm o,in}}\, e^{i\omega_{\rm o}t} \begin{bmatrix} e^{i\phi(t)} - e^{-i\phi(t)} \\ ie^{i\phi(t)} + ie^{-i\phi(t)} \end{bmatrix}. \tag{2}$$

We arbitrarily choose $E_1(t)$ as the propagated field and calculate the optical power at the link output as

$$P_{\rm o,out}(t) = \frac{\alpha_{\rm link}E_1^*(t)E_1(t)}{2\kappa^2} = \frac{1}{2}\alpha_{\rm link}\alpha_{\rm mzm}P_{\rm o,in}\left[1 - \cos(2\phi(t))\right] \tag{3}$$

where $\alpha_{\rm link}$ is the link optical power loss factor.

The total photocurrent is calculated using the definition $I(t) \equiv \Re P_{\rm o,out}$, where $\Re$ is the photodiode responsivity in A/W. Inserting this into (3) and expanding yields

$$I(t) = \frac{1}{2}\Re\alpha_{\rm link}\alpha_{\rm mzm}P_{\rm o,in}\left[1 - \cos(\phi_{\rm dc})\cos(\phi_{\rm rf}\sin\Omega t) + \sin(\phi_{\rm dc})\sin(\phi_{\rm rf}\sin\Omega t)\right]. \tag{4}$$

Next, we define $\zeta \equiv \left(\Re \alpha_{\text{link}} \alpha_{\text{mzm}} P_{\text{o,in}}\right)/2$ and use the identities $\cos(x\sin\theta) = J_0(x) + 2\sum_{\text{n}=1}^{\infty} J_{2\text{n}}(x)\cos(2\text{n}\theta)$ and $\sin(x\sin\theta) = 2\sum_{\text{n}=0}^{\infty} J_{2\text{n}+1}(x)\sin[(2\text{n}+1)\theta]$, where J_{m} is the m$^{\text{th}}$-order Bessel function of the first kind, to rewrite (4) as

$$\begin{aligned} I(t) = \zeta\left[1 - \cos(\phi_{\text{dc}})J_0(\phi_{\text{rf}})\right] - 2\zeta\cos(\phi_{\text{dc}})\sum_{\text{n}=1}^{\infty} J_{2\text{n}}(\phi_{\text{rf}})\cos(2\text{n}\Omega t) \\ + 2\zeta\sin(\phi_{\text{dc}})\sum_{\text{n}=0}^{\infty} J_{2\text{n}+1}(\phi_{\text{rf}})\sin[(2\text{n}+1)\Omega t] \end{aligned} . \tag{5}$$

Equation (5) is a very important result. The first term describes a DC component, the second RF components at even harmonics of the modulation frequency and the third RF components at the fundamental frequency and odd harmonics. The weighting of these components can be controlled, at least in part, by adjusting the DC bias. For example, the MZM can be biased at "peak" when $\phi_{\text{dc}} = (2k + 1)\pi$, "null" when $\phi_{\text{dc}} = 2k\pi$ or "quadrature" when $\phi_{\text{dc}} = (2k + 1)\pi/2$ (k is an integer). With the MZM at quadrature, (5) becomes

$$I(t) = I_{\text{dc}} + 2I_{\text{dc}}\sum_{\text{n}=0}^{\infty} J_{2\text{n}+1}(\phi_{\text{rf}})\sin[(2\text{n}+1)\Omega t] \tag{6}$$

where we have identified the DC photocurrent as $I_{\text{dc}} = \zeta$. Given the signal photocurrent in (6), we can then calculate the RF output power at the fundamental frequency as $P_{\text{rf,out}} = \left(I_{\Omega}^2 Z_{\text{out}}\right)/2$ where I_{Ω} is the coefficient of the analog term at angular frequency Ω and Z_{out} is the output impedance of the link. Using this definition we have

$$P_{\text{rf,out}} = 2I_{\text{dc}}^2 J_1^2(\phi_{\text{rf}})Z_{\text{out}} . \tag{7}$$

Given the RF output power (7), we can now calculate the RF gain using the definitions $G_{\text{rf}} \equiv P_{\text{rf,out}}/P_{\text{rf,in}}$ and $P_{\text{rf,in}} \equiv V_{\text{rf}}^2/(2Z_{\text{in}})$ where Z_{in} is the input link impedance. The RF gain is then

$$G_{\text{rf}} = \frac{4I_{\text{dc}}^2 J_1^2(\phi_{\text{rf}})Z_{\text{in}}Z_{\text{out}}}{V_{\text{rf}}^2} . \tag{8}$$

Most often, the small-signal gain, that is, the gain in the linear operating regime, is the most important. This region is defined by the inequality $V_{\text{rf}} << V_{\pi}$, or equivalently, $\phi_{\text{rf}} << 1$. This condition allows us to use the approximation $J_{\text{m}}(\phi_{\text{rf}}) \approx \phi_{\text{rf}}^{\text{m}}/(2^{\text{m}}\,\text{m}!)$ to write the small-signal gain as

$$G_{\text{rf,ss}} = \left(\frac{I_{\text{dc}}}{V_{\pi}}\right)^2 \pi^2 Z_{\text{in}}Z_{\text{out}} \tag{9}$$

where we have also used the definition of ϕ_{rf}. In Fig. 4, $G_{rf,ss}$ is plotted as a function of I_{dc}, showing a photonic link can exhibit gain and in that sense act as an RF amplifier. It is of particular importance to note that $G_{rf} \propto I_{dc}^2 \propto P_{o,in}^2 = P_{laser}^2$, where P_{laser} is the laser output power. The considerations in terms of optimizing gain in an IMDD link therefore include the amount of laser power available, the insertion loss of the entire link, power handling of the components (especially the photodiode) and the V_π of the MZM. The first three considerations aim at maximizing I_{dc}; there are tradeoffs between MZM insertion loss and V_π that must be considered. However, as with any RF component or system, the noise performance and linearity of an IMDD link must be considered along with the gain.

The noise in an analog photonic link is of particular importance in the derivation of RF noise figure (NF_{rf}), compression dynamic range (CDR) and spurious-free dynamic range (SFDR). There are three sources of noise in an unamplified analog photonic link: thermal noise, detector shot noise and laser noise. (Noise associated with optical amplification is treated in detail in [8]-[11].) Thermal or Johnson noise [12] is a spectrally white noise associated with a resistor in thermal equilibrium. For matched resistors in thermal equilibrium at a temperature T, the thermal noise power spectral density delivered from one resistor to the other is $k_B T$ where k_B is Boltzmann's constant. For an analog photonic link, thermal noise is present at the link input and the link output. The noise power spectral density at the link output due to thermal noise at the link input is given by

$$N_{ith} = G_{rf,ss} k_B T \tag{10}$$

where $G_{rf,ss}$ is given by (9). Equation (10) describes thermal noise at the link input that is modulated onto the laser and in that sense is a signal that sees the link gain. The thermal noise power spectral density delivered from the link output to a matched load is

$$N_{oth} = k_B T \, . \tag{11}$$

Like thermal noise, detector shot noise [13] is spectrally white. The mean squared shot noise current spectral density at the link output is given by $i_{sh}^2 = 2eI_{dc}$ where e is the electronic charge constant (taken to be positive) and I_{dc} is again the DC photocurrent. Given i_{sh}^2 the noise power spectral density at the link output due to shot noise is

$$N_{sh} = 2eI_{dc}Z_{out} \, . \tag{12}$$

The noise due to the transmit laser in a photonic link cannot be written analytically. The laser noise spectrum in the RF domain at the link output depends on the specific laser; sources of noise include the relaxation oscillation, spontaneous emission, mode-competition, cavity instability, loss fluctuations, and pump instability. Laser noise is typically specified as relative intensity noise (RIN). In terms of noise power spectral density due to a laser at the link output, N_{laser}, the RIN for a laser is

$$RIN_{laser} = \frac{N_{laser}}{I_{dc}^2 Z_{out}} \, , \tag{13}$$

that is, the noise power spectral density associated with the laser relative to the DC power at the link output. For reasons that will soon be apparent, it is quite useful to treat all of the noise sources in terms of RIN. Therefore, we define the total output-referenced generalized relative

intensity noise as $RIN_{\text{total}} \equiv N_{\text{total}} / \left(I_{\text{dc}}^2 Z_{\text{out}} \right)$ where N_{total} is the total output noise power spectral density. At this point, $N_{\text{total}} = N_{\text{laser}} + N_{\text{ith}} + N_{\text{sh}} + N_{\text{oth}}$ and we can therefore write the RIN contributions for the remaining noise sources as

$$RIN_{\text{ith}} = \frac{\pi^2 k_{\text{B}} T Z_{\text{in}}}{V_\pi^2} \tag{14}$$

$$RIN_{\text{oth}} = \frac{k_{\text{B}} T}{I_{\text{dc}}^2 Z_{\text{out}}} \tag{15}$$

$$RIN_{\text{shot}} = \frac{2e}{I_{\text{dc}}} \tag{16}$$

where we have used (10)-(12). From here, we will derive the remaining RF metrics in terms of RIN_{total}.

The noise figure of an analog link is the degradation in signal-to-noise ratio incurred through the link and is defined as $NF_{\text{rf}} \equiv SNR_{\text{in}} / SNR_{\text{out}}$ where SNR_{in} and SNR_{out} are the signal-to-noise ratios at the input and output of the link, respectively. We can rewrite NF_{rf} as $NF_{\text{rf}} = S_{\text{in}} N_{\text{total}} / \left(N_{\text{in}} S_{\text{out}} \right) = G_{\text{rf}} N_{\text{out}} / N_{\text{in}}$, where S_{in} and S_{out} are the input and output signal powers, respectively, and N_{in} is the input noise power spectral density. Strictly, NF_{rf} is a function of S_{in} in the sense that G_{rf} is not linear. However, NF_{rf} as a metric is typically assumed to be defined under small-signal drive. Given this assumption, we can use (9) and the definition of RIN_{total} to write

$$NF_{\text{rf}} = \frac{RIN_{\text{total}} V_\pi^2}{\pi^2 k_{\text{B}} T Z_{\text{in}}} \tag{17}$$

where we have assumed a thermally-limited input. The calculated noise figure for IMDD is shown in Fig. 4 as a function of I_{dc}. In Fig. 4, NF_{rf} is shown with no RIN_{laser} and for various values of RIN_{laser}, demonstrating that laser noise can significantly limit the performance of an analog photonic link below what is fundamentally possible.

In addition to gain and noise figure, the linearity of an RF device or system must be considered. The two most-commonly-used metrics to describe linearity are CDR and SFDR. The CDR is defined as the range of input powers over which the output power is above the noise floor and not more than 1-dB compressed. This concept is shown geometrically in Fig. 2, where data from an IMDD link are employed. Using Fig. 2 it is straight-forward to see that CDR is defined in logarithmic form as $\text{CDR}(\text{dB} \cdot \text{Hz}) = P_{\text{rf,out}}^{\text{1dB}}(\text{dBm}) + 1 - N_{\text{total}}(\text{dBm/Hz})$ or in linear units as

$$\text{CDR} \equiv \frac{10^{0.1} P_{\text{rf,out}}^{\text{1dB}}}{N_{\text{total}}} \tag{18}$$

where $P_{\text{rf,out}}^{\text{1dB}}$ is the RF output power at 1-dB compression. Note that as defined here, CDR is normalized to a 1-Hz bandwidth and to obtain the unit-less CDR, (18) must be divided by the bandwidth. The SFDR for analog systems or components is defined as the range of input powers over which the signal is above the noise floor and all spurious signals (distortion) are below the

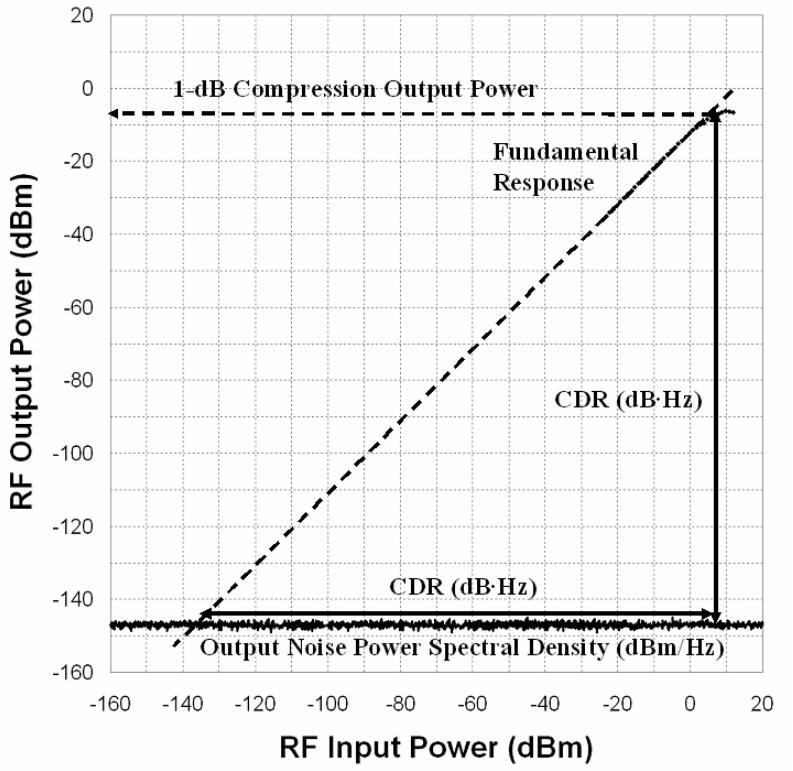

Fig. 2. The definition of compression dynamic range (CDR), shown geometrically using data from an intensity-modulation direct-detection link. Shown is measured RF output power as a function of RF input power, from which the CDR can be defined as the range of input powers over which 1) the signal is above the noise floor and 2) the signal is at worst 1-dB compressed.

noise floor. Again, it is instructive to view the definition of SFDR in a geometrical sense as is shown in Fig. 3. The data used in Fig. 3 are from an IMDD link, where, as we will see, the highest-order distortion is a third-order term. The definition for SFDR is, however, given in arbitrary-order as $\mathrm{SFDR}\left(\mathrm{dB}\cdot\mathrm{Hz}^{(n-1)/n}\right)\equiv(n-1)\left(OIPn(\mathrm{dBm})-N_{\mathrm{total}}(\mathrm{dBm/Hz})\right)/n$, where n is the order of the largest distortion and $OIPn$ is the n^{th}-order intercept, defined as the intercept of the linear extrapolations of the fundamental and distortion response (see Fig. 3). In linear units

$$\mathrm{SFDR}=\left(\frac{OIPn}{N_{\mathrm{total}}}\right)^{(n-1)/n}, \tag{19}$$

which is again normalized to a 1-Hz bandwidth. We will now derive CDR and SFDR for an IMDD architecture.

The CDR is derived for an IMDD link by using (7) to calculate $P_{\mathrm{rf,out}}^{\mathrm{1dB}}$. The linear approximation of (7) gives $P_{\mathrm{rf,out}}^{\mathrm{1dB}}$ as

$$10^{0.1}P_{\mathrm{rf,out}}^{\mathrm{1dB}}=\frac{1}{2}I_{\mathrm{dc}}^{2}\phi_{\mathrm{rf}}^{2}Z_{\mathrm{out}}\Big|_{\phi_{\mathrm{rf}}=\phi_{\mathrm{1dB}}} \tag{20}$$

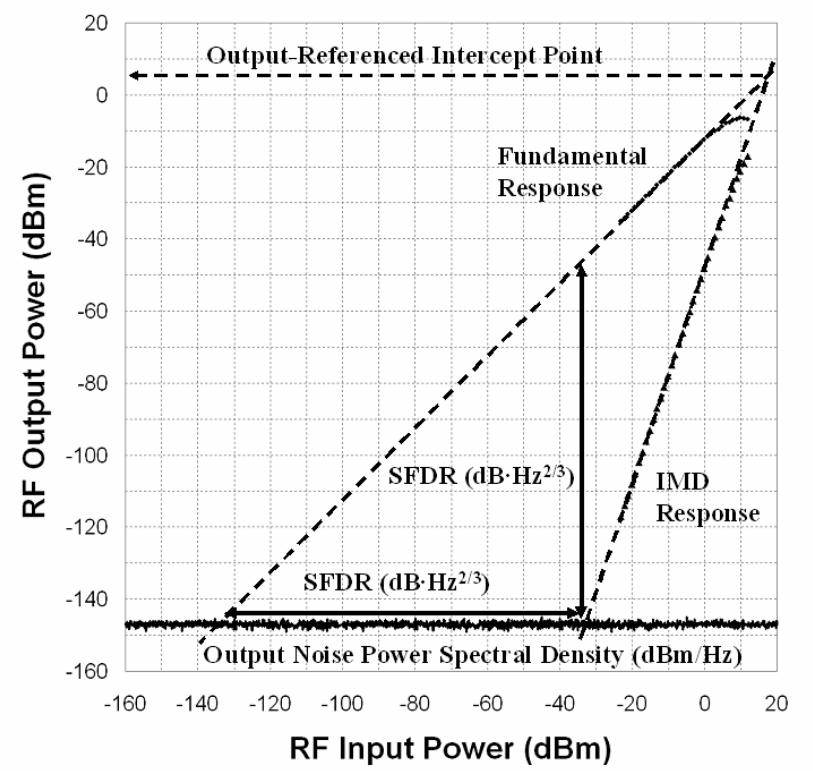

Fig. 3. The geometrical definition of spurious-free dynamic range (SFDR) for a third-order distortion. The SFDR is defined as the range of input powers over which 1) the signal is above the noise floor and 2) the all spurious signals and intermodulation distortion (IMD) are below the noise floor.

where $\phi_{1\text{dB}}$ is the phase shift amplitude at the 1-dB compression point. The condition used to calculate $\phi_{1\text{dB}}$ is given by

$$\frac{\phi_{1\text{dB}}}{J_1(\phi_{1\text{dB}})} = 2\times 10^{0.05} \tag{21}$$

which can be solved numerically to yield $\phi_{1\text{dB}} \approx 0.9504$. The CDR is then obtained by inserting (20) into (18) and using the definition of RIN_{total} to obtain

$$\text{CDR} = \frac{\phi_{1\text{dB}}^2}{2RIN_{\text{total}}}. \tag{22}$$

The CDR for an IMDD link is plotted against I_{dc} in Fig. 4, again showing that RIN_{laser} can severely limit the performance.

To derive the SFDR, an expression for the highest-order distortion must be obtained. Of particular importance is intermodulation distortion, that is, distortion that is present under multi-tone driving of an analog system or component. The standard used to quantify this type of distortion is the two-tone test. The two-tone test comprises two equal-amplitude drive signals spaced by a small frequency difference. To model a two-tone test for an analog photonic system, we evaluate (3) with $\phi(t)$ rewritten as $\phi(t) = \phi_{\text{dc}}/2 + (\phi_{\text{rf}}/2)\sin\Omega_1 t + (\phi_{\text{rf}}/2)\sin\Omega_2 t$. With a

quadrature bias ($\phi_{dc} = \pi/2$) and after some algebra, we obtain the following photocurrent for this modulation

$$\begin{aligned} I_{2-\text{tone}}(t) = I_{dc} &+ 2I_{dc}J_0(\phi_{rf})\sum_{k=0}^{\infty} J_{2k+1}(\phi_{rf})\sin[(2k+1)\Omega_1 t] \\ &+ 2I_{dc}J_0(\phi_{rf})\sum_{m=0}^{\infty} J_{2m+1}(\phi_{rf})\sin[(2m+1)\Omega_2 t] \\ &+ 2I_{dc}\sum_{k=0}^{\infty}\sum_{l=1}^{\infty} J_{2k+1}(\phi_{rf})J_{2l}(\phi_{rf})\sin[2l\Omega_2 t \mp (2k+1)\Omega_1 t] \\ &+ 2I_{dc}\sum_{m=0}^{\infty}\sum_{n=1}^{\infty} J_{2m+1}(\phi_{rf})J_{2n}(\phi_{rf})\sin[2n\Omega_1 t \mp (2m+1)\Omega_2 t] \end{aligned} . \quad (23)$$

To determine the *OIPn*, we take the small-signal approximation of (23) ($J_m(\phi_{rf}) \approx \phi_{rf}^m / (2^m m!)$), which yields

$$I_{2-\text{tone,ss}}(t) = I_{dc} + I_{dc}\phi_{rf}\sin(\Omega_{1,2}t) + \frac{I_{dc}\phi_{rf}^3}{8}\sin(2\Omega_{2,1}t \mp \Omega_{1,2}t) . \quad (24)$$

The second set of terms in (24) are the response at the fundamentals and the third set of terms are the largest distortions, third-order terms. We look to determine *OIP*3 by taking the intersection of the RF output power associated with the fundamental and third-order distortion, given by the equality $I_{dc}^2\phi_{rf}^2 Z_{out}/2 = I_{dc}^2\phi_{rf}^6 Z_{out}/128$. This expression gives $\phi_{rf,OIP3} = 2\sqrt{2}$, which can be inserted into the linear expression for the fundamental power (7) to give the *OIP*3 as

$$OIP3 = I_{dc}^2\phi_{rf,OIP3}^2 Z_{out}/2 = 4I_{dc}^2 Z_{out} . \quad (25)$$

Given the *OIP*3, we use (19) and the definition of RIN_{total} to write the SFDR for an IMDD link as

$$\text{SFDR} = \left(\frac{4}{RIN_{total}}\right)^{2/3} . \quad (26)$$

The SFDR for an IMDD link is plotted as a function of I_{dc} in Fig. 4, showing decreased SFDR for increased RIN_{laser}.

We have shown that laser noise can severely limit the performance of analog photonic links in terms of the NF_{rf}, CDR and SFDR performance metrics. In addition, G_{rf} is shown to depend directly on the laser output power. These statements are quantitatively demonstrated in Fig. 4, where equations (9), (17), (22) and (26) are used. The form of these equations explicitly shows the dependence on RIN_{laser}, demonstrating that if $RIN_{laser} >> RIN_{shot} + RIN_{ith} + RIN_{oth}$, optimal performance will not be achieved. As a reference, the analytical equations used in calculating link performance are given in logarithmic form in the Appendix. No analytical expression is given for the laser noise because it is a measured quantity specific to each laser. In the following section, we describe the experimental technique used to measure laser noise.

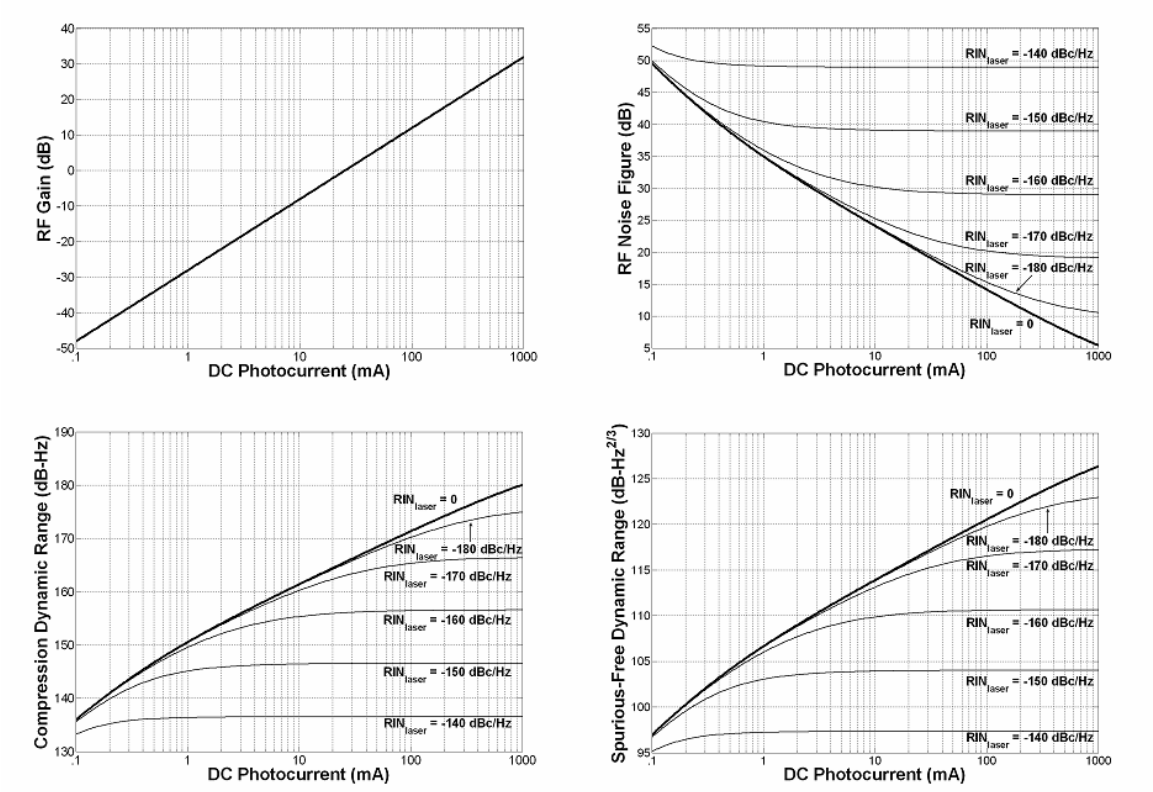

Fig. 4. The calculated performance metrics for an analog photonic link employing intensity modulation with direct detection as functions of DC photocurrent. Shown are RF gain, RF noise figure, compression dynamic range and spurious free dynamic range calculated using equations (9), (17), (22) and (26), respectively. Here $V_\pi = 5$ V, $T = 293$ K and $Z_{in} = Z_{out} = 50\ \Omega$ were used. In each case, the bold black represents the fundamentally-limited performance, excluding laser noise. The RF gain is shown not to depend on laser noise but does depend on laser output power. The remaining three performance metrics are demonstrated to depend heavily on laser relative intensity noise (RIN_{laser}), which can severely limit the performance below the fundamental limits.

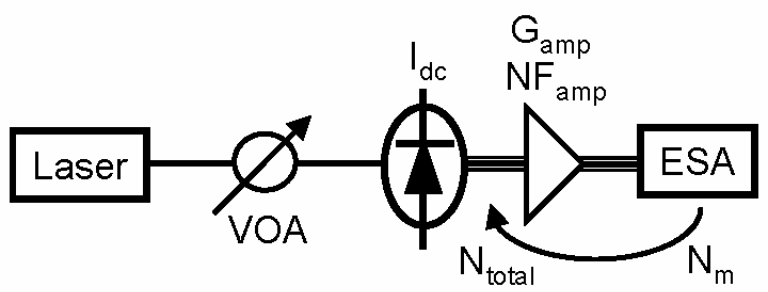

Fig. 5. The experimental setup for measuring laser noise in an intensity-modulation direct-detection system. A laser is attenuated with a variable optical attenuator (VOA) and detected with a photodiode at a DC photocurrent I_{dc}. The total noise at the photodiode output N_{total} is amplified by a radio-frequency amplifier with gain G_{amp} and noise figure NF_{amp}. The measured noise N_m is obtained as a function of radio frequency using an electrical spectrum analyzer (ESA), from which N_{total} can be calculated.

3 NOISE MEASUREMENT METHODOLOGY

In this section we will describe the methodology for measuring the laser noise in an IMDD system employing some laser. We will describe the experimental procedure along with the calculation used to interpret the experimental results. The experimental setup for the noise measurement is shown in Fig. 5. The laser under test is set to the desired output power and then attenuated using a variable optical attenuator (VOA) to a power that provides a suitable DC photocurrent. Here, "suitable DC photocurrent" means the highest photocurrent that is available with the laser power at hand and/or the highest photocurrent that the photodiode can linearly handle. Typically the total RF noise at the photodiode output N_{total} is well below the noise floor of the electrical spectrum analyzer (ESA) used for the measurement. Therefore, an RF amplifier with enough gain G_{amp} and low enough noise figure NF_{amp} must be employed to amplify the noise, which is measured on the ESA as N_m. Typically, G_{amp} is measured using a network analyzer. A good check on the measurement system is to perform the following steps. 1) Measure the noise power spectral density on the ESA terminated in 50 Ω, this is the noise floor of the ESA. 2) Measure the noise power spectral density of the amplifier terminated in 50 Ω (N_{amp}), this is the amplified thermal noise plus the additional noise due to the amplifier. This noise power spectral density should be higher then that in Step 1 by a few dB. 3) Measure the noise power spectral density with the photodiode connected and the laser on, this is N_m. Again, this noise power spectral density should be higher that than in Step 2 by a few dB. (A set of measurements representative of Steps 1, 2 and 3 are shown in Fig. 6.) 4) Finally, an RF attenuator should be placed between the photodiode and the amplifier to ensure that the amplifier is not compressed. Given the measured parameters, N_m, G_{amp}, N_{amp} and I_{dc}, we can calculate the RIN as follows.

First the amplifier noise figure can be calculated as $NF_{amp} = N_{amp} / \left(G_{amp} k_B T \right)$. Because the measurements involved are typically done on a logarithmic scale, it is instructive to write the logarithmic form of this equation and those that follow. For the amplifier noise figure we have

$$NF_{amp}\left[\text{dB}\right] = N_{amp}\left[\text{dBm/Hz}\right] - G_{amp}\left[\text{dB}\right] + 173.9 \tag{27}$$

where $T = 293$ K was used. With NF_{amp} given by (27) we can back out N_{total} from N_m as

$$N_{total}\left[\text{dBm/Hz}\right] = 10\log\left(\frac{N_m\left[\text{mW/Hz}\right]}{g_{amp}} - nf_{amp} \times 10^{-17.39} \right) \tag{28}$$

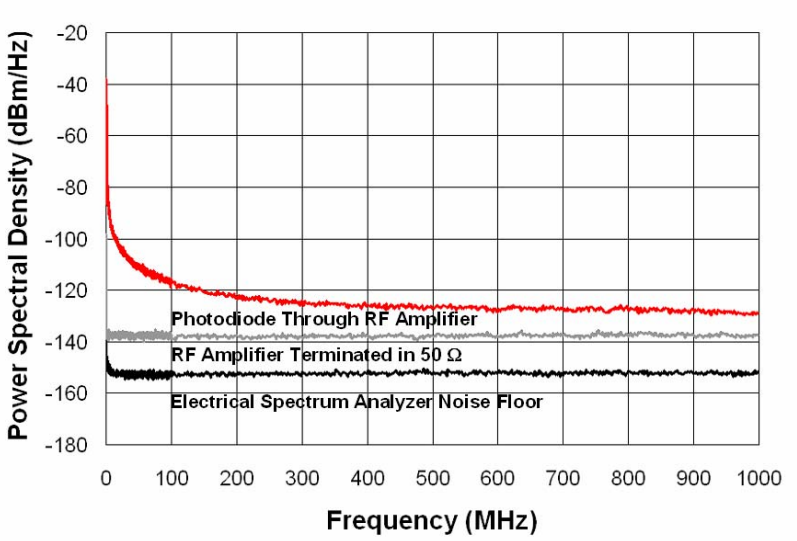

Fig. 6. Example of the testing procedure for a noise measurement setup. First, the electrical analyzer noise floor is measured (black). The noise power spectral density of the radio-frequency amplifier terminated in 50 Ω is then measured (grey) and ensured to be a few dB above the electrical amplifier noise floor, more than 10 dB in this case. Finally, the noise power spectral density with the optics in place is measured (red), which again should be a few dB above the noise in the previous step.

where g_{amp} and nf_{amp} are meant to signify where linear terms for the amplifier gain and noise figure must be used. From N_{total} we can then calculate the RIN as

$$RIN\left[\text{dBc/Hz}\right] = 13 + N_{\text{total}}\left[\text{dBm/Hz}\right] - 20\log\left(I_{\text{dc}}\left[\text{mA}\right]\right). \tag{29}$$

It is important to note here that the definition of RIN (29) assumes that all of the RF power is delivered from the photodetector to the RF amplifier. In actuality, many photodetectors have an impedance-matching circuit built into their packaging, typically matched to 50 Ω. As shown in Fig. 7, such an impedance-matched system acts as an RF-current divider for an AC-coupled load. If we want to reference the measured noise to the DC photocurrent there is a 6-dB correction to (29) that results in

$$RIN\left[\text{dBc/Hz}\right] = 19 + N_{\text{total}}\left[\text{dBm/Hz}\right] - 20\log\left(I_{\text{dc}}\left[\text{mA}\right]\right) \quad \text{(with matched load).} \tag{30}$$

We therefore have two equations, (29) and (30), that allow us to calculate the RIN for the system shown in Fig. 5. These RIN values include RIN_{shot} and RIN_{oth} but not RIN_{ith} (there is no modulator in the noise measurement system). As shown in Fig. 8 we can plot the minimum RIN for the system shown in Fig. 5 as a function of DC photocurrent. The calculated data in Fig. 8 are applicable to a matched or unmatched detector and puts a limit on the measurable RIN_{laser}. In other words, for, say, I_{dc} = 10 mA, RIN_{min} = –165 dBc/Hz and a $RIN_{\text{laser}} << -165$ dBc/Hz cannot be measured. We will see more of these types of examples in the following section where measured data are analyzed.

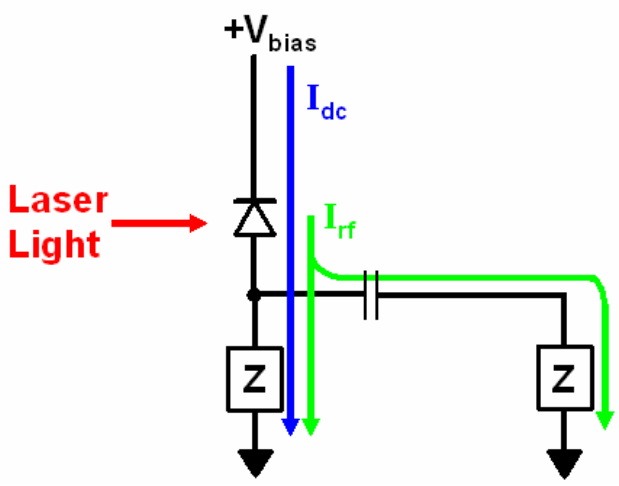

Fig. 7. Schematic of a photodiode with an impedance-matching circuit connected to an AC-coupled load. Shown are the path of the measured DC photocurrent in blue and the path of the RF photocurrent in green. Only half of the generated RF photocurrent is delivered to the load and for noise-power-spectral-density measurements relative to the DC photocurrent, a 6-dB correction must be used as in Equation (30).

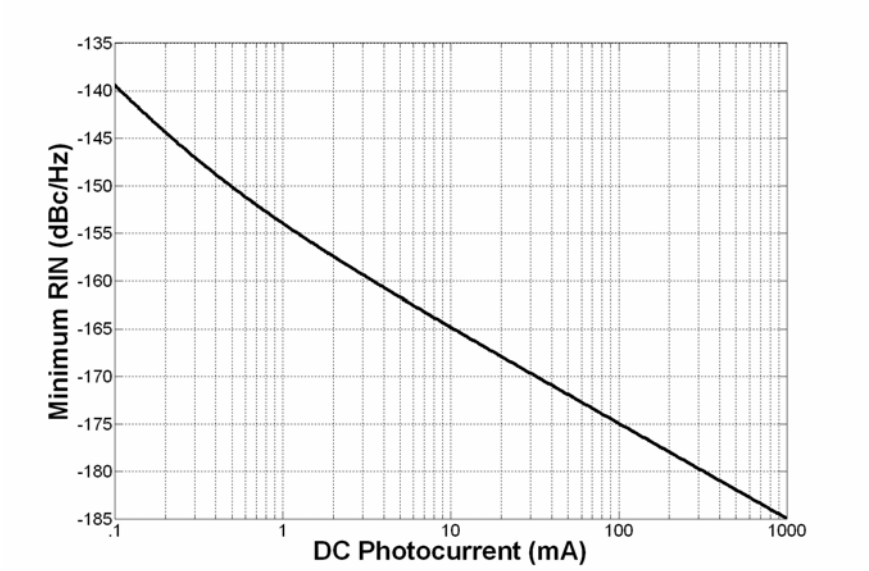

Fig. 8. The calculated minimum relative intensity noise in the measurement system shown in Fig. 5 as a function of DC photocurrent. The relative intensity noise due to output thermal noise (Equation 15) and shot noise (Equation 16) are considered here. The third fundamental noise source in an analog photonic link, input thermal noise, is not considered here because the measurement system in Fig. 5 does not contain a modulator. Laser relative intensity noise at a particular DC photocurrent cannot be measured much below the minimum relative intensity noise plotted above.

4 LASER NOISE SPECTRA

Using the methodology described in Section 3, we present and discuss the measurement results for various lasers suitable for use in analog photonic systems. We start with the data in Fig. 9, which shows the measured RIN spectrum for a Lightwave Electronics Nd-YAG laser (Model No. M125N-1319-200, Serial No. 2628, low-noise rebuild) with approximately 230 mW output power at about 1320 nm. For these data, and in all that follow, the ESA employed was an Agilent 8563EC. For the data in Fig. 9 a custom detector [14] was employed and I_{dc} = 80 mA, to the authors' knowledge the highest photocurrent at which laser noise measurements have been made. As shown by the location of the electrical noise floor, no RF amplifier was required for these measurements. Of note in the Nd-YAG RIN spectrum is the peak due to the relaxation oscillation at about 300 kHz and the significant suppression of this peak using the RIN-suppression option available from the vendor. The RIN-suppression circuit reduces noise at and below the peak but does cause a small rise in noise above 700 kHz, as opposed to the intrinsic operation of the laser. The peaks in the RIN spectrum below 100 kHz are not attributed to the laser itself but to electrical noise in the laser-controller electronics. It is expected that these peaks can be removed by sourcing the required pump current with, for example, batteries. The peak in the spectrum at about 8.5 GHz is due to a competing mode in the laser cavity, spaced by that frequency in the optical domain. Save this sidemode peak, $RIN_{laser} << RIN_{shot} = -173.9$ dBc/Hz above 70 MHz and we can say that the laser is shot-noise-limited at I_{dc} = 80 mA in this region. (As mention in Section 3 and described by Fig. 8, it is very important to state the DC photocurrent at which a laser is "shot noise limited." This is often overlooked in the literature and especially by laser vendors. For example, to state that "a 1550-nm 1-W laser is shot noise limited" without stating the photocurrent implies that $RIN_{laser} << -185.9$ dBc/Hz, the shot noise limit for an ideal detector with 1-W of 1550-nm light on it. Because a measurement at this photocurrent is unachievable, the preceding claim is nonsensical.) The noise above 70 MHz in excess of the RIN_{shot} limit in Fig. 9 is due to the fact that the detector used has no impedance-matching circuit, which results in resonances due to impedance mismatch. As a verification of this claim, we show in Fig. 10 that the measured response of the detector in an IMDD architecture closely follows the measured noise spectrum. It is worth noting here that the RIN spectra shown in this report, calculated using (29) or (30), include RIN_{laser} and RIN_{shot}. This point is demonstrated explicitly in Fig. 9, using the intrinsic Nd-YAG data. At 300 kHz, RIN_{laser} dominates whereas at 70 MHz RIN_{shot} dominates. The transition from these two limiting regions occurs above 10 MHz. Therefore, the calculation to extract RIN_{laser} near 15 MHz where RIN = −170 dBc/Hz goes as $RIN_{laser} = 10\log\left(10^{-17} - 10^{-17.39}\right) = -172.3$ dBc/Hz . It is more instructive to include RIN_{shot} in the measured data and including RIN_{shot} serves as an additional check on the measurement system.

The Nd-YAG laser is a good laser for analog photonic links and is often used as a reference because of its low noise and high output power. Furthermore, at frequencies above 70 MHz and away from 8.5 GHz, fundamentally-limited performance is available at any presently feasible DC photocurrent. However, in systems where optical amplification must be employed, the 1320-nm wavelength of the Nd-YAG is undesirable. This wavelength is outside the bandwidth of erbium-doped fiber amplifiers (EDFAs), the most robust and proven optical amplifiers. It is therefore desirable to operate near 1550 nm, where various other solid-state-laser technologies are available. We present the RIN spectra for the main candidates in Fig. 11 for frequencies up to 1 GHz, noting that the RIN spectra are quite similar at higher frequencies. Shown are data for an older-vintage Nd-YAG laser at 230 mW (Lightwave Electronic M125N-1319-200, pre-low-noise

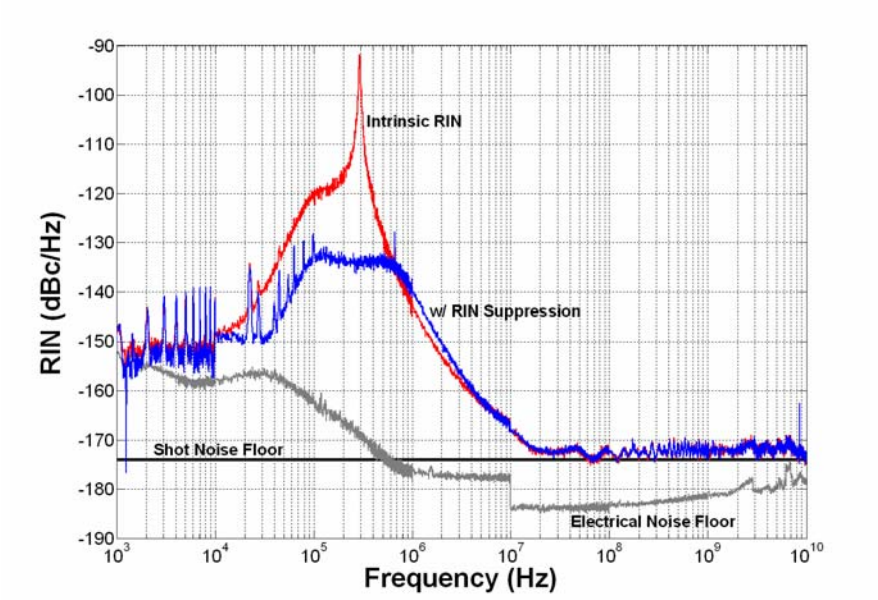

Fig. 9. The measured RIN spectrum for a Lightwave Electronics Model No. M125N-1319-200 (Serial No. 2628) Nd-YAG solid-state laser. The laser output power is approximately 230 mW at 1320 nm and the DC photocurrent was 80 mA for the measurement. Shown is the electrical noise floor (grey) and the calculated shot noise floor at −173.9 dBc/Hz (bold black). The measured laser data show the RIN with the manufacturer's RIN-suppression circuitry employed (blue) and the RIN spectrum without RIN suppression (red).

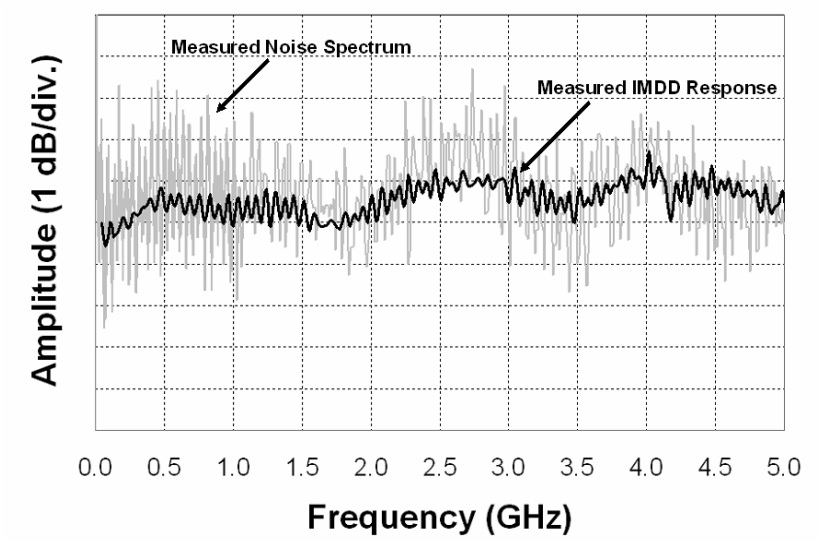

Fig. 10. The measured noise spectrum data from Fig. 9 (grey) plotted against the measured intensity-modulation with direct-detection (IMDD) response (black) for the detector employed in the noise measurement. These data confirm that the frequency characteristic of the noise at high frequencies is dominated by the response of the detector and not due to the laser itself.

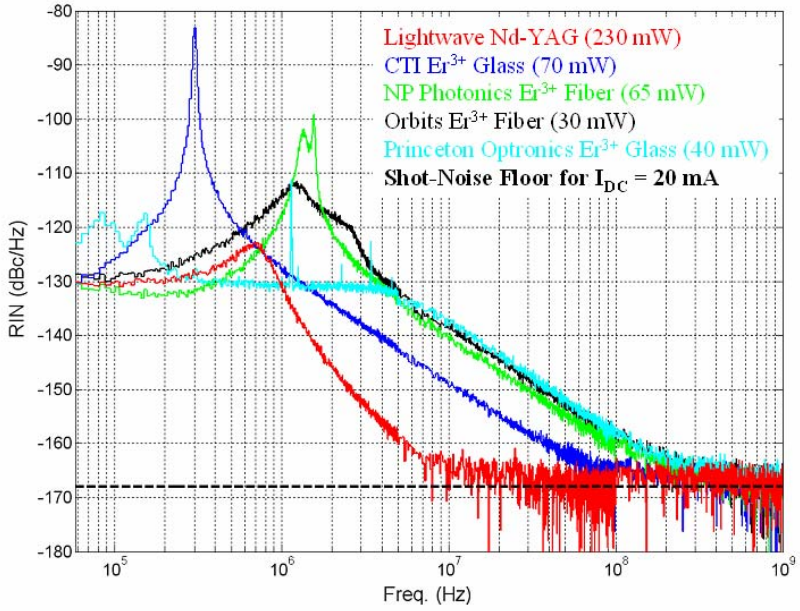

Fig. 11. The measured RIN spectra for solid-states lasers at 20 mA DC photocurrent, resulting in a shot noise floor at −168 dBc/Hz (dashed black). Shown are data for a Lightwave Electronics Nd-YAG in red (Model No. M125N-1319-200, pre-low-noise-rebuild), a CLR/CTI Photonics Er^{3+}-doped-glass laser in blue (METEOR® Model, Serial No. 72), an NP Photonics Er^{3+}-doped-fiber laser in green (Model SMPF-2030, Serial No. D-89-030619-07), an Orbits Lightwave Er^{3+}-doped-fiber laser in black (Model 2800A, Serial No. 001033) and a Princeton Optronics Er^{3+}-doped-glass laser in teal (Model BC4001, Serial No. 325).

rebuild, $\Delta\nu \sim 8.5$ GHz), an Er^{3+}-doped-glass laser at 70 mW (CLR/CTI Photonics METEOR®, Serial No. 72, $\Delta\nu \sim 24$ GHz), an Er^{3+}-doped-fiber laser at 65 mW (NP Photonics SMPF-2030 Serial No. D-89-030619-07, $\Delta\nu \sim 2$ GHz), an Er^{3+}-doped-fiber laser at 30 mW (Orbits Lightwave 2800A Serial No. 001033, $\Delta\nu \sim 1.7$ GHz) and an Er^{3+}-doped-glass laser at 40 mW (Princeton Optronics BC4001 Serial No. 325, $\Delta\nu \sim 55$ GHz). Here, the $\Delta\nu$ designates the approximate mode-spacing of the laser and indicates that a spurious signal will exist in the RF domain at that frequency. All lasers except the Nd-YAG are at about 1550 nm and all of the data were measured at $I_{dc} = 20$ mA. The 20-mA photocurrent results in a shot noise floor at −168 dBc/Hz. The photodetector used in these experiments was a Discovery Semiconductor DSC50 and the RF amplifier a Sonoma Instrument 310. Note that all of the lasers are shot noise limited by 600 MHz for this photocurrent, making all of them suitable for microwave photonics applications. The Nd-YAG is obviously superior for unamplified applications, having the highest output power and the lowest noise above 1 MHz. Another advantage of these lasers is their intrinsically low linewidth as compared to commercial semiconductor lasers. As shown in Fig. 12, the measured linewidth for a solid-state laser can be orders of magnitude smaller than a semiconductor laser. This linewidth advantage is of particular importance for coherent applications but has no impact on IMDD systems. In addition, typical semiconductor lasers are smaller and cheaper than the solid-state lasers shown above. Because they are used in commercial telecommunications, where the noise requirements are not as stringent as in an analog system, semiconductor lasers exhibit better manufacturability and more robustness than present solid-state technologies. We therefore must consider the performance of such lasers, especially in comparison to that of the competing solid-state lasers above.

The RIN spectrum for a commercial semiconductor distributed feedback (DFB) laser (JDS CQF 938, Serial No. 477844) is shown in Fig. 13 against some solid-state lasers at the same 20-mA photocurrent. Here, the same photodiode and RF amplifier as those used for the data in Fig.

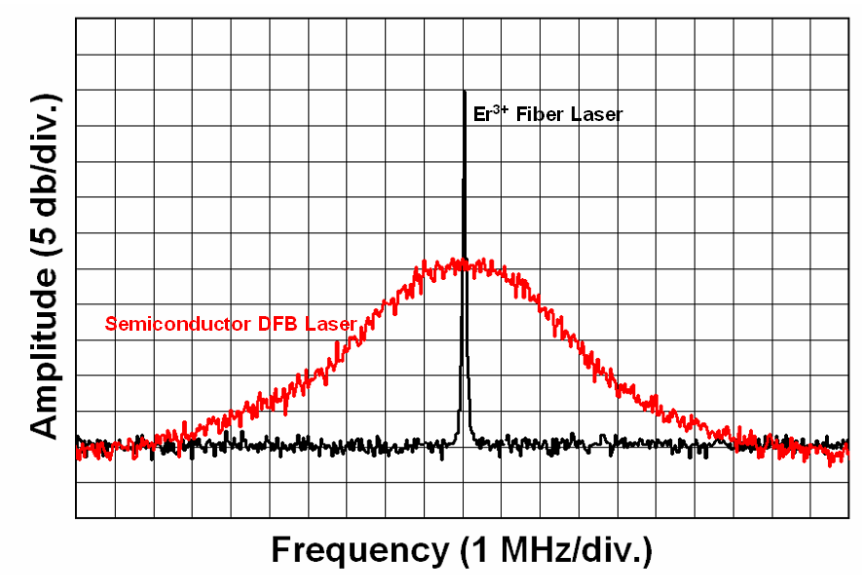

Fig. 12. The measured linewidth spectra for an Er^{3+}-doped-fiber solid state laser against that for a semiconductor distributed feedback (DFB) laser. The latter has a linewidth on the order of a couple of MHz whereas the former exhibits a linewidth of about 2.5 kHz.

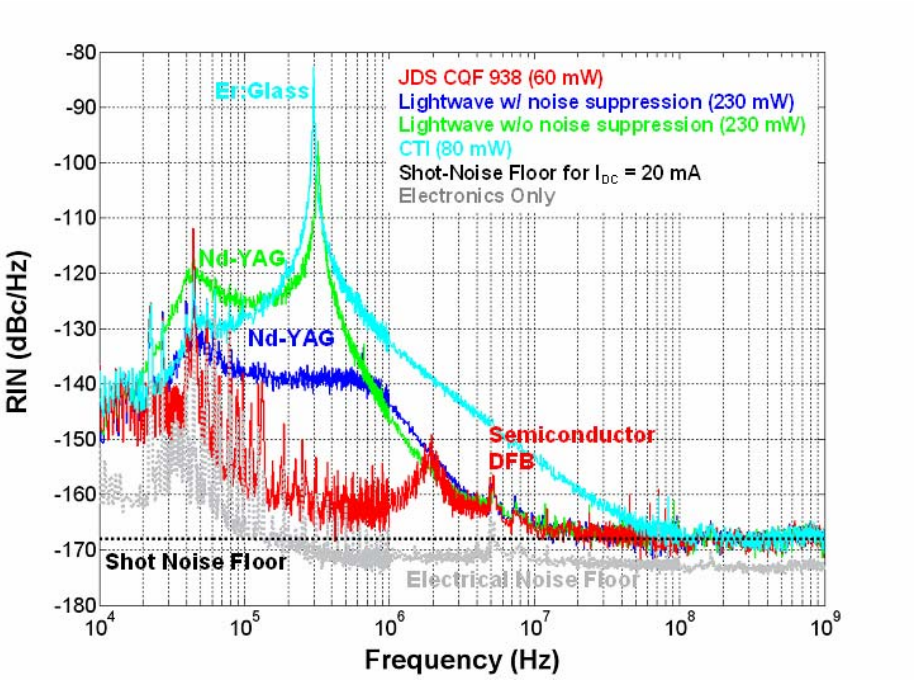

Fig. 13. The measured relative intensity noise spectrum for a semiconductor laser compared to those for some solid-state lasers. Shown in grey is the electrical noise floor and in dashed black the shot noise floor for I_{dc} = 20 mA at –168 dBc/Hz. Relative intensity noise spectra are plotted for a semiconductor distributed feedback laser in red (JDS CQF 938, Serial No. 477844), a Lightwave Electronics Nd-YAG without noise suppression in green (Model No. M125N-1319-200, post-low-noise-rebuild), the same Nd-YAG with noise suppression in blue, and an Er^{3+}-doped-glass laser in teal (CLR/CTI Photonics METEOR® Model, Serial No. 72). The peak in the semiconductor spectrum near 20 MHz is attributed to the laser drive electronics.

11 were employed. At frequencies below 100 MHz, the DFB laser exhibits significantly less RIN than the solid-state lasers. In fact, save the noise near 20 MHz due to the laser driver, the DFB laser noise is limited by shot noise or the electrical measurement system noise. It does have less output power than the solid-state architectures but as we will shortly see, semiconductor technology has advanced to the point where competing output powers are now available. We therefore see that for applications well below 1 GHz, a semiconductor DFB offers a lower-noise solution than a solid state laser.

The RIN spectra for the four major semiconductor DFB lasers are plotted in Figs. 14 and 15. The lasers that were measured are a JDS CQF 938/600 (Serial No. 477838) at 63 mW with a wavelength $\lambda \sim 1550$ nm and a pump current $I_p = 340$ mA, an EM4 EM253 (Serial No. A06050001) at 90 mW with $\lambda \sim 1550$ nm and $I_p = 400$ mA, an Ortel 1772 (Serial No. F065957) at 64 mW with $\lambda \sim 1550$ nm and $I_p = 300$ mA, and an EM4 EM273 (Serial No. E0002232) at 175 mW with $\lambda \sim 1320$ nm and $I_p = 1000$ mA. The latter has the most power but again suffers from the impracticality that its wavelength is out of band for optical amplification with an EDFA. The data in Fig. 14 show the RIN spectra from 10 kHz to 1 GHz at $I_{dc} = 20$ mA ($RIN_{shot} = -168$ dBc/Hz). For these data a Discovery Semiconductor DSC50S photodetector and a Sonoma Instrument 310 RF amplifier were employed. The higher-frequency data shown in Fig. 15 was obtained using a Discovery Semiconductor DSC30S photodiode at $I_{dc} = 10$ mA ($RIN_{shot} = -165$ dBc/Hz) and a Miteq AFS4-00102650-42-10P-44 RF amplifier. The low-noise spectra are quite similar for each laser, with differing structure due to the drive electronics. Again, the noise peaks would most likely be removed with a carefully-designed low-noise current source. More interestingly, the high-frequency plots show that each laser exhibits a different relaxation oscillation frequency and therefore different peaks in their RIN spectra. We list the approximate peaks in the RIN due to laser as: 1) JDS 938/600: $RIN_{laser,peak} = -167$ dBc/Hz near 15 GHz, 2) EM4 EM253: $RIN_{laser,peak} = -165$ dBc/Hz near 8 GHz, 3) Ortel 1772: $RIN_{laser,peak} = -163$ dBc/Hz near 15 GHz, and 4) EM4 EM273: $RIN_{laser,peak} = -157$ dBc/Hz at 20 GHz. Note first that these values are for RIN_{laser}, extracted as explained above, and therefore do not match the total RIN values in Fig. 15 and secondly that the EM4 EM273 RIN_{laser} may continue to rise above 20 GHz. The data presented in these plots will allow one to calculate analog system performance as a function of frequency for an IMDD system employing each laser. Equations (A.2)-(A.4) give RF noise figure (given V_π), compression dynamic range and spurious-free dynamic range where RIN_{total} can be taken from Figs. 14 and 15. Note that RIN_{total}, as given by Figs. 14 and 15 does not include RIN_{ith} but that RIN_{ith} is often negligible. (Given a particular V_π, (A.5) should be employed to verify this.) Finally, given a particular DC photocurrent, limited by the available laser power, the gain is given by (A.1).

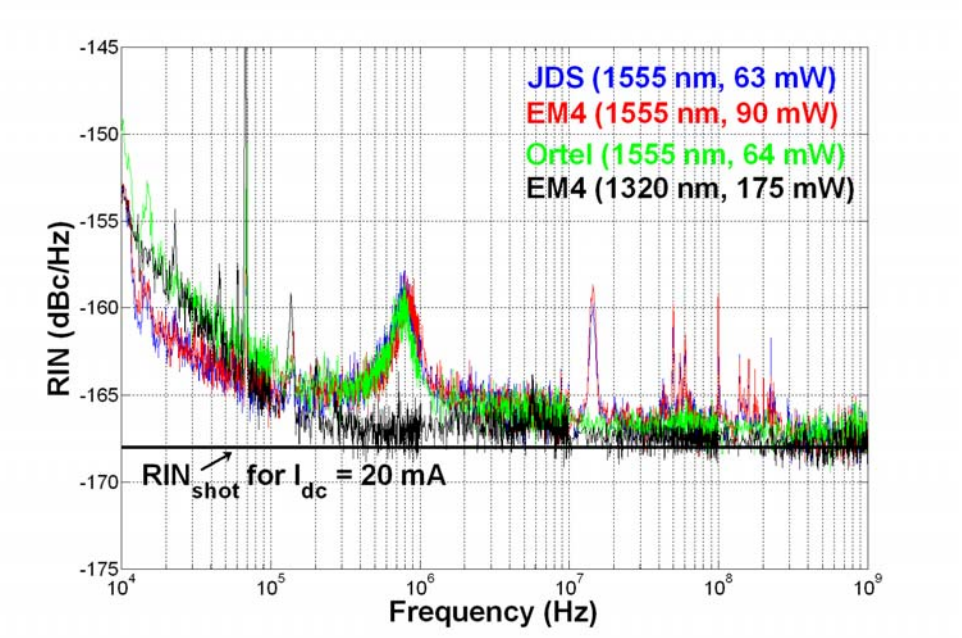

Fig. 14. The measured relative intensity noise spectra for several semiconductor distributed feedback lasers. . Shown in bold black is the shot noise floor for I_{dc} = 20 mA at –168 dBc/Hz. Relative intensity noise spectra are plotted for JDS CQF 938/600 (Serial No. 477838) with a wavelength λ ~ 1550 nm and a pump current I_p = 340 mA (blue), an EM4 EM253 (Serial No. A06050001) with λ ~ 1550 nm and I_p = 400 mA (red), an Ortel 1772 (Serial No. F065957) with λ ~ 1550 nm and I_p = 300 mA (green), and an EM4 EM273 (Serial No. E0002232) with λ ~ 1320 nm and I_p = 1000 mA (black).

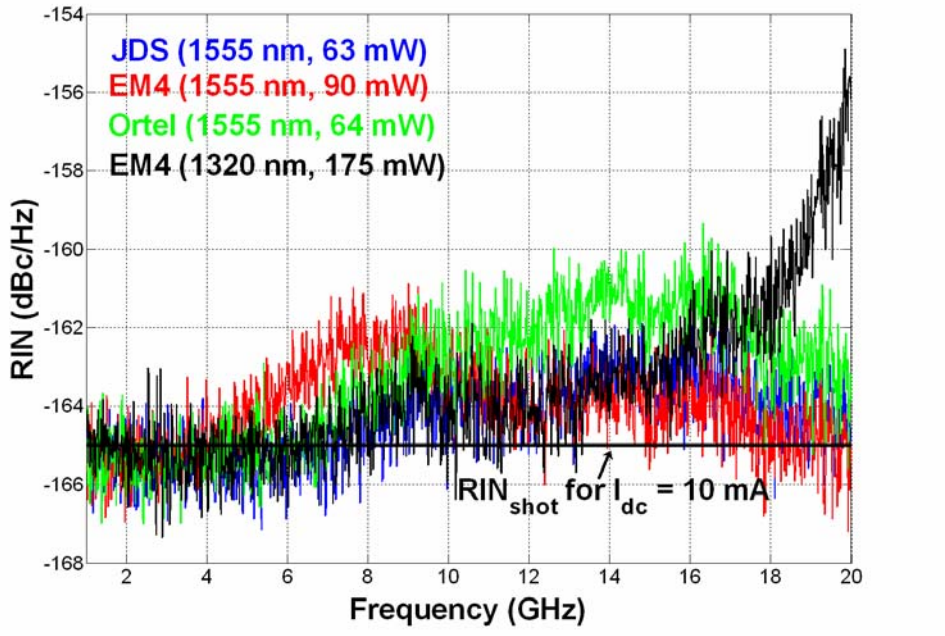

Fig. 15. The measured relative intensity noise spectra for the same lasers in Figure 14 with the same color coding but at higher frequencies. Because a smaller photodiode was required, a lower photocurrent of I_{dc} = 10 mA was achieved, which gives RIN_{shot} = –165 dBc/Hz.

5 SUMMARY AND CONCLUSIONS

We have presented a derivation of the performance metrics for an intensity-modulation direct-detection analog photonic architecture, specifically detailing the impairments imposed by laser noise. The equations in Section 2 provide a sound theoretical foundation for the understanding of analog photonics. These equations, along with those given in the Appendix can be used to calculate analog link performance from simple relative intensity noise measurements, given the half-wave voltage of the Mach-Zehnder modulator. The methodology for such relative intensity noise measurements has been demonstrated in sufficient detail such that anyone with a rudimentary background in experimental analog photonics should be able to complete the measurements. We have also presented measured relative intensity noise data using the competing solid-state and semiconductor laser technologies. The former represent relatively un-commercialized lasers as compared to the time-proven semiconductor distributed feedback design. The most significant experimental results of this report for immediate system design are given in Figures 14 and 15. These figures give the relative intensity noise spectra for the four major commercially-available semiconductor lasers in the frequency range of 10 kHz to 20 GHz. We note that while these lasers are the most important for presently- and soon-to-be-deployed analog photonic systems, we are of the opinion that solid-state laser technology will be extremely important in the future of analog photonics.

APPENDIX: LOGARITHMIC FORMS OF IMDD EQUATIONS

The logarithmic forms of selected equations from Section 2 are given here. First, the RF gain for an IMDD link is given by (9) as

$$G_{\mathrm{rf}}[\mathrm{dB}] = -16.1 + 20\log\left(I_{\mathrm{dc}}[\mathrm{mA}]\right) - 20\log\left(V_{\pi}[\mathrm{V}]\right) \tag{A.1}$$

where $Z_{\mathrm{in}} = Z_{\mathrm{out}} = 50\ \Omega$ was used. The remaining IMDD performance metrics, RF noise figure, compression dynamic range and spurious-free dynamic range are given by equations (17), (22) and (26) as

$$NF_{\mathrm{rf}}[\mathrm{dB}] = 176.9 + 20\log\left(V_{\pi}[\mathrm{V}]\right) + RIN_{\mathrm{total}}[\mathrm{dBc/Hz}] \tag{A.2}$$

$$\mathrm{CDR}[\mathrm{dB\cdot Hz}] = -3.5 - RIN_{\mathrm{total}}[\mathrm{dBc/Hz}] \tag{A.3}$$

$$\mathrm{SFDR}\left[\mathrm{dB\cdot Hz^{2/3}}\right] = 4.0 - \frac{2}{3} RIN_{\mathrm{total}}[\mathrm{dBc/Hz}] \tag{A.4}$$

which depend on $RIN_{\mathrm{total}} = RIN_{\mathrm{ith}} + RIN_{\mathrm{oth}} + RIN_{\mathrm{shot}} + RIN_{\mathrm{laser}}$. As discussed in the report, there is no analytical expression for RIN_{laser}. We use equations (14)-(16) with $T = 293$ K to obtain

$$RIN_{\mathrm{ith}}[\mathrm{dBc/Hz}] = -176.9 - 20\log\left(V_{\pi}[\mathrm{V}]\right) \tag{A.5}$$

$$RIN_{\mathrm{oth}}[\mathrm{dBc/Hz}] = -160.8 - 20\log\left(I_{\mathrm{dc}}[\mathrm{mA}]\right) \tag{A.6}$$

$$RIN_{\text{shot}}\left[\text{dBc/Hz}\right] = -154.9 - 10\log\left(I_{\text{dc}}\left[\text{mA}\right]\right) \tag{A.7}$$

These equations (A.1)-(A.7), along with the measured RIN_{laser}, can then be used to quickly determine the performance of an IMDD analog photonic system.

REFERENCES

[1] E. E. Funk, V. J. Urick, and F. Bucholtz, "High dynamic range, long haul (>100 km) radio over fiber," in *Microwave Photonics*, C. H. Lee (editor), CRC Press, pp. 185-212, 2007.

[2] E. I. Ackerman and A. S. Daryoush, "Broad-band external modulation for fiber-optic links for antenna remoting applications," *IEEE Trans. Microwave Theory Tech.*, vol. 45, no. 8, pp. 1436-1442.

[3] X. S. Yao, "Optoelectronic oscillators," in *RF Photonic Technology in Optical Fiber Links*, W. S. C. Chang (editor), Cambridge University Press, New York, 2002.

[4] J. Capmany, B. Ortega, D. Pastor, and S. Sales, "Discrete-time optical processing of microwave signals," *J. Lightwave Technol.*, vol. 23, no. 2, pp. 702-723, Feb. 2005.

[5] J. D. McKinney and A. M. Weiner, "Compensation of the effects of antenna dispersion on UWB waveforms via optical pulse-shaping techniques," *IEEE Trans. Microwave Theory Tech.*, vol. 54, no. 4, pp. 1681-1686.

[6] G. C. Tavik, C. L. Hilterbrick, J. B. Evans, J. J. Alter, J. G. Crnkovich Jr., J. W. de Graaf, W. Habicht II, G. P. Hrin, S. A. Lessin, D. C. Wu, and S. M. Hagewood, "The advanced multifunction RF concept," *IEEE Trans. Microwave Theory Tech.*, vol. 52, no. 3, pp. 1009-1020, Mar. 2005.

[7] A. L. Campillo, E. E. Funk, D. A. Tulchinsky, J. L. Dexter, and K. J. Williams, "Phase performance of an eight-channel wavelength-division-multiplexed analog-delay line," *J. Lightwave Technol.*, vol. 22, no. 2, pp. 440-447, Feb. 2004.

[8] V. J. Urick, F. Bucholtz, and K. J. Williams, "Noise penalty of highly-saturated erbium-doped fiber amplifiers in analog links," *IEEE Photon. Technol. Lett.*, vol. 18, no. 6, pp. 749-751, Mar. 2006.

[9] V. J. Urick, F. Bucholtz, and K. J. Williams, "Correction to 'Noise penalty of highly-saturated erbium-doped fiber amplifiers in analog links,'" *IEEE Photon. Technol. Lett.*, vol. 18, no. 13, pp. 1475, July 2006.

[10] V. J. Urick, M. S. Rogge, F. Bucholtz, and K. J. Williams, "The performance of analog photonics links employing highly-compressed erbium-doped fiber amplifiers," *IEEE Trans. Microwave Theory Tech.*, vol. 54, no. 7, pp. 3141, 3145, July 2006.

[11] V. J. Urick, F. Bucholtz, and K. J. Williams, "Optically-amplified short-length analog photonic links," *IEEE Topical Meeting on Microwave Photonics*, Grenoble, France, paper W2.2, Oct. 2006.

[12] P. Horowitz and W. Hill, "The Art of Electronics," 2nd ed., New York, Cambridge, pp. 430-431, 1989.

[13] W. V. Sorin, "Noise sources in optical measurements," in *Fiber optic test and measurement*, D. Derickson (editor), Prentice Hall, Upper Saddle River, pp. 597-613, 1998.

[14] D. A. Tulchinsky, X. LI, N. Li, S. Demiguel, J. C. Campbell, and K. J. Williams, "High-saturation current wide-bandwidth photodetectors," *IEEE J. Selected Topics Quantum Electron.*, vol. 10, no. 4, pp. 702-708, 2004.